Towards inferring earthquake patterns from geodetic observations of interseismic coupling

Yoshihiro Kaneko[1]*, Jean-Philippe Avouac[2] and Nadia Lapusta[2,3]

Ultimately, seismotectonic studies seek to provide ways of assessing the timing, magnitude and spatial extent of future earthquakes. Ample observations document the spatial variability in interseismic coupling, defined as a degree of locking of a fault during the period of stress build-up between seismic events: fully or nearly locked fault patches are often surrounded by aseismically creeping areas. However, it is unclear how these observations could help assess future earthquakes. Here we simulate spontaneous seismic and aseismic fault slip with a fully dynamic numerical model. Our simulations establish the dependence of earthquake rupture patterns and interseismic coupling on spatial variations of fault friction. We consider the long-term evolution of slip on a model fault where two seismogenic, locked segments are separated by an aseismically slipping patch where rupture is impeded. We find that the probability for a large earthquake to break through the rupture-impeding patch is correlated with the interseismic coupling averaged over this patch. In addition, the probability that an earthquake breaks through the rupture-impeding patch and interseismic coupling are both related to fault friction properties through a single non-dimensional parameter. Our study opens the possibility of predicting seismic rupture patterns that a fault system can produce on the basis of observations of its interseismic coupling, and suggests that regions of low interseismic coupling may reveal permanent barriers to large earthquakes.

Simple conceptual models of fault behaviour assume that seismic rupture segmentation is persistent and that fault segments remain locked in the interseismic period separating episodic slip events[1]. These models predict quasiperiodic repetition of 'characteristic' earthquakes with similar rupture extent and moment[2] or a time-predictable or slip-predictable behaviour if non-quasiperiodic behaviour is allowed[1]. As observations accumulate, it becomes quite evident that earthquake sequences on natural faults are more complex than these simple models predict[3–6], although faults do seem to obey some systematic behaviours with respect to their segmentation[7] and, possibly, the timing of major earthquakes[8]. One potential explanation is that faults may consist of several subsegments that rupture either independently or jointly with neighbouring segments during larger earthquakes[7,9], with the non-periodic or even chaotic behaviour arising from stress transfers and their effect on prestress[10–12]. This segmentation may partly be controlled by geometrical complexities such as local non-planarity and fault step-overs[13]. However, there is growing evidence that spatial variation of fault friction properties is an influential and perhaps determining factor that affects the spatial extent, size and timing of earthquake ruptures. Hence, barriers prone to aseismic creep may have an important effect on the observed patterns of seismic ruptures, an issue that is the focus of this study.

Evidence for heterogeneous fault friction properties

Measurements of surface deformation show that, in the interseismic period between successive large earthquakes, some fault areas remain locked whereas others creep aseismically. This has been observed along a number of subduction zones including Sumatra, Japan, Alaska, Peru and Chile[14–19]. The pattern of interseismic coupling (ISC), the ratio of slip deficit during the interseismic

period divided by the long-term slip (Supplementary Information S2), is thus generally found to be heterogeneous and, to some degree, coincides with the pattern of large earthquakes. For example, the distribution of seismic asperities in the Kurile–Japan trench seems to be relatively stationary[20] and lie within a zone with high ISC (ref. 21). Similarly, large earthquakes offshore of Sumatra seem to have ruptured areas that had remained locked during the interseismic period[6,16]. More evidence that the mode of slip on faults varies spatially comes from observations of aseismic afterslip occurring in areas surrounding the seismic ruptures[19,22–25] and seismic patches embedded in creeping faults in various tectonic settings[15,26,27].

These observations can be interpreted as evidence for heterogeneous fault friction properties. In the laboratory, both rock surfaces and layers of fault gouge have been shown to exhibit rate and state frictional behaviour (Supplementary Information S1), in which the steady-state frictional strength τ_{ss} can be expressed as[28,29]

$$\tau_{ss} = \bar{\sigma}\left[f_0 + (a-b)\ln(V/V_0)\right] \qquad (1)$$

where a and b are rate and state parameters, V is slip rate, f_0 and V_0 are the reference friction coefficient and slip rate and $\bar{\sigma}$ is the effective normal stress. In steady state, rock friction exhibits either velocity weakening (VW, $a-b < 0$) or velocity strengthening (VS, $a-b > 0$), depending on a number of factors including normal stress, temperature and the type of rock material[28–32]. Models predict that VS fault regions would slip stably under slow tectonic loading, whereas VW fault regions would produce 'stick–slip' motion[12,33–38].

In this framework, earthquakes and aseismic slip are mainly linked to VW and VS segments, respectively, although earthquakes can penetrate into VS segments and parts of VW segments can

---

[1]Institute of Geophysics and Planetary Physics, Scripps Institution of Oceanography, University of California, La Jolla, California 92093, USA, [2]Division of Geological and Planetary Sciences, California Institute of Technology, Pasadena, California 91125, USA, [3]Division of Engineering and Applied Science, California Institute of Technology, Pasadena, California 91125, USA. *e-mail: ykaneko@ucsd.edu.
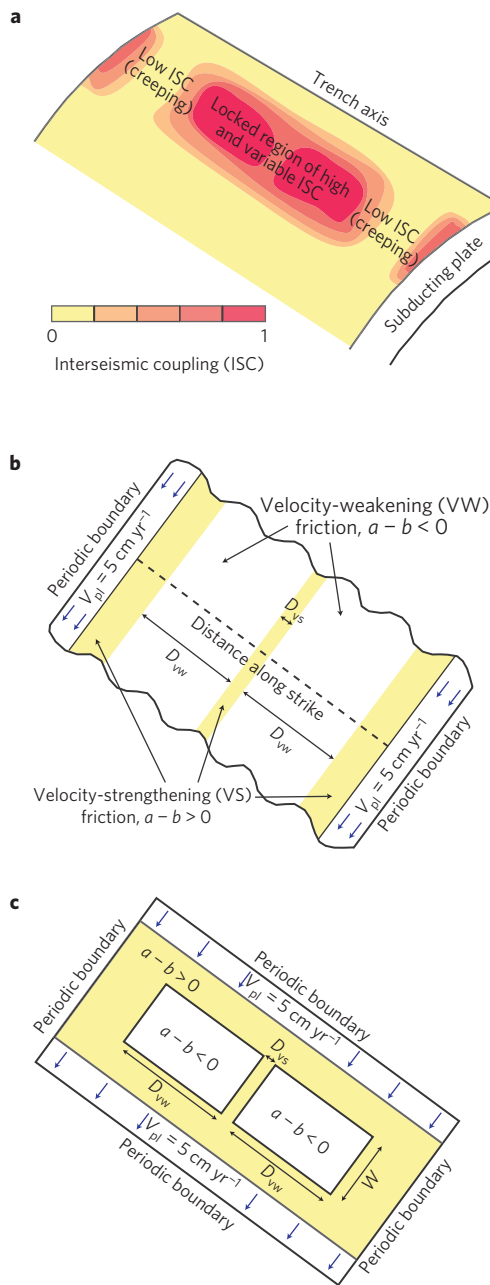
Figure 1 | Schematic illustrations of ISC as commonly observed on subduction megathrust faults and distribution of friction properties in our 2D and 3D models. a, The proportion of slip accommodated by interseismic creep varies spatially, from 0% in fully locked areas (ISC = 1) to 100% in areas creeping with the interplate rate (ISC = 0). **b**, The 2D model is intended to investigate the effect of friction heterogeneity in the along-strike direction. **c**, The 3D model has the same along-strike heterogeneity of friction properties at the seismogenic depth as the 2D model but incorporates a finite seismogenic fault width W.

experience aseismic slip[37,39–41]. Fault patches that creep aseismically can be interpreted to be dominantly VS whereas locked patches are dominantly VW. Predominantly creeping patches that are characterized by a VS frictional behaviour can act as systematic barriers to earthquake propagation, as in the case of the Batu Islands area, Sumatra[16], or in the Paracas Peninsula area, Southern Peru[19]. On the other hand, some earthquakes rupture across aseismic barriers. For example, the 1964 Alaska earthquake of moment magnitude M_w 9.2 ruptured through an area with locally low

ISC (ref. 42). The impeding effect of this patch may have been responsible for the two-peaked source-time function[43]. Similarly, the 2007 Pisco earthquake ruptured two locked patches separated by a VS barrier[19,44]. Patches with relatively low ISC, but not as pronounced as in the Batu Islands, are also observed in the Mentawai Islands[16] and presumably influenced the 2007 earthquake sequence[6]. The non-systematic effect of these heterogeneities on seismic ruptures might be the origin of the complex behaviour of this area, which repeatedly involved clustered large earthquakes with overlapping rupture areas[8]. Together, these observations imply that spatial variations of fault friction properties can influence the location and extent of seismic ruptures in a systematic or non-systematic manner. However, how such variations translate into the pattern of ISC and complexity of earthquake ruptures is not well understood. To explore this issue, we construct fault models that contain variations in friction properties.

Model of earthquake cycles with heterogeneous coupling

We use numerical experiments to explore the effect of VS patches on ISC and on the seismic rupture pattern over many earthquake cycles. Our model contains a planar fault governed by the ageing form of rate and state friction[28,29] and embedded in a homogeneous elastic medium (Supplementary Information S1). The fault has two identical VW segments separated and surrounded by VS regions. In the simpler two-dimensional (2D) implementation, we consider only along-strike variations (Fig. 1b), which enables us to assess a broad range of model behaviour as the parameters are varied. Several calculations in a three-dimensional (3D) model (Fig. 1c) are conducted to check the validity of the findings derived from the 2D simulations. The fault is loaded by imposing a constant slip velocity outside the simulated region. The friction properties and lengths of the fault segments are varied to study their effect on the model behaviour. Fault slip is simulated using a unique methodology[37,45] that resolves all stages of seismic and aseismic slip: the aseismic nucleation process, the subsequent inertially controlled earthquakes with realistic slip rates and rupture speeds, the postseismic slip and the interseismic deformation between earthquakes.

Realistic earthquake behaviour produced by the model

Despite the simple geometry and distribution of friction properties, the model produces rich earthquake behaviour similar to that of natural faults. A 2D simulation example is shown in Fig. 2 (Supplementary Movie S1 gives a 3D simulation example). The VW segments are nearly fully locked in the interseismic period (ISC ≈ 1) and slip mostly during seismic events. Some earthquakes rupture only a fraction of a VW segment (for example, events 3–5 in Fig. 2b); they arrest because of lower prestress caused by previous slip (Fig. 3). Other events grow large and sometimes propagate through the VS patch. The large VS regions of low ISC on both sides of the model act as permanent barriers to coseismic slip. The central VS patch affects local ISC and acts as a barrier during some coseismic ruptures (for example, events 6, 14 and 25 in Fig. 2b). In the example of Fig. 2, 83% and 10% of the total slip in the VS patch is accumulated seismically and as afterslip, respectively (Fig. 2f). This example shows that a region of nearly uniform and high ISC can have significant variations in friction properties, resulting in complex rupture patterns (Fig. 2).

The VS patch causes clustering of large events and overlapping rupture areas. When only one of the VW segments ruptures, stress is transferred to the neighbouring VW segment owing to the coseismic static stress change and afterslip, leading to event clustering: the two VW segments tend to rupture much closer in time than their recurrence periods (Fig. 2c). After such one-segment ruptures, stress increase in the VS patch promotes propagation of the subsequent large earthquake through the patch. The slightly VS patch gradually relieves the transient stress
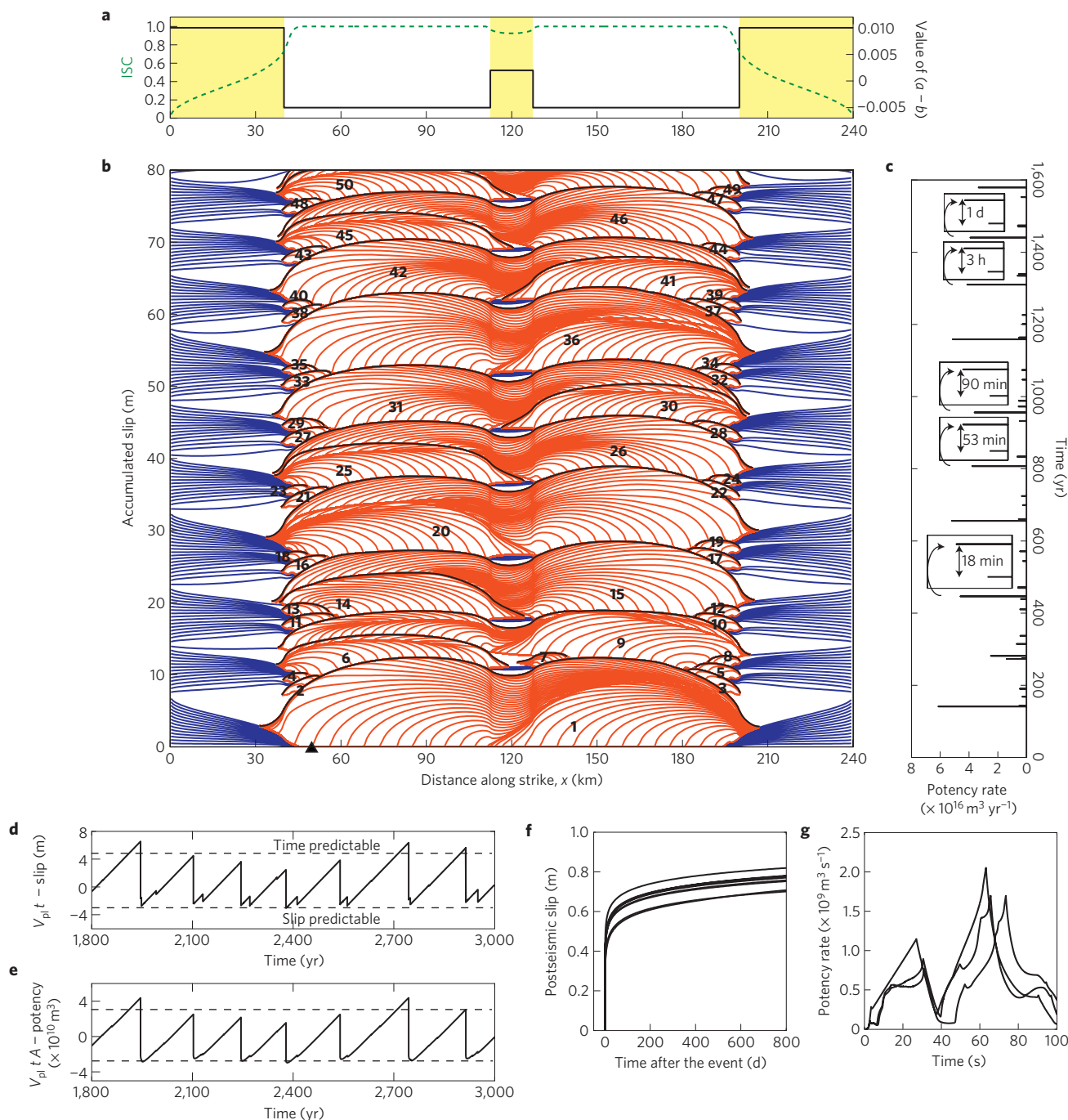
Figure 2 | An example of long-term fault behaviour computed in the 2D model. a, The assigned distribution of the friction parameter $(a − b)$ (solid line) results in a small VS patch between two VW segments, which appear as a single area of high and slightly variable ISC (dashed line) (Supplementary Information S2). In this example, the VS patch results in a locally lower ISC, but the effect is subtle (ISC = 0.93). **b**, Contours of slip accumulated over 1,600 yr show that the VS patch creates complexity of large earthquakes within what seems to be a locked area of high ISC. Red, blue and black lines show slip accumulation every 2 s during the simulated earthquakes, every 10 yr and after each earthquake, respectively. Numbers indicate earthquakes in the order of their occurrence. **c**, Potency rate over time (a downdip width of 40 km is assumed). Insets show close-up views of clustered successive events. **d**, Time evolution of slip deficit at one VW point ($x = 50$ km) indicated by a triangle in **b**. Dashed lines illustrate that the model is neither time nor slip predictable. **e**, Potency deficit over the entire fault. **f**, Afterslip computed at the centres of the VS patch ($x = 120$ km) after events 1, 9, 15, 20, 26, 31, 36 and 42, which all propagated through the VS patch. **g**, Potency rates of events 1, 20 and 36 show that the VS patch results in double-peaked source-time functions.

increase by afterslip, but the stress level often remains high at the time of the next large earthquake, promoting rupture propagation through the patch. Hence a VS patch within a well-locked zone can be identified as a place where nearby ruptures tend to overlap, with the second rupture being generally larger than the first one. For example, event 6 (Fig. 2b) ruptures only the left VW segment and then event 9 is able to rupture both VW segments eight years later. This behaviour may explain the overlapping rupture areas of the 1797 M_w 8.8 and 1833 M_w 9.0 earthquakes in Sumatra.
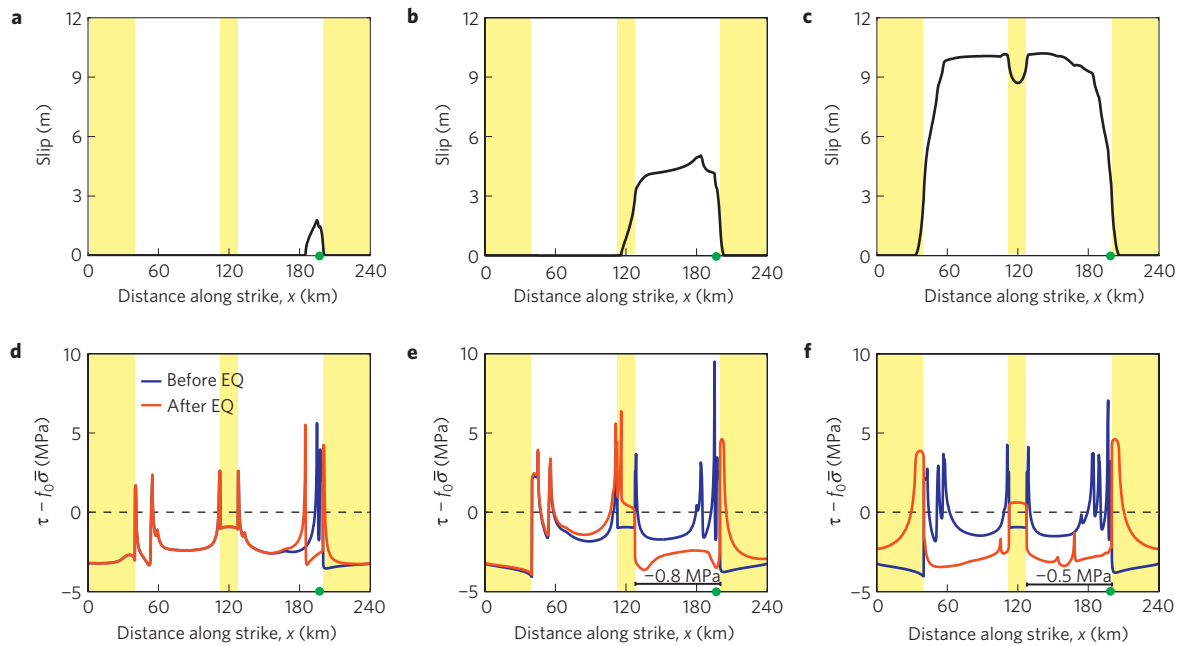
365

Figure 3 | Characteristics of simulated earthquakes and causes of rupture arrest. a–c, Coseismic slip distributions for three representative, earthquakes (events 28, 30 and 36 in Fig. 2b) including an event that arrests in the VS patch (**b**) and an event that propagates through the patch (**c**). **d–f,** The corresponding distributions of shear stress τ before and after the earthquakes, with respect to a reference stress value $f_0\bar{\sigma}$. We define the beginning/end of an earthquake as the time when the maximum slip rate V_{max} on the fault reaches/decreases below $1\,cm\,s^{-1}$. Epicentres are marked by green dots. Coseismic static stress drops are in the range of 1–10 MPa, typical for natural earthquakes.

For a wide range of parameters, our model does not produce characteristic earthquakes, nor does it obey the slip-predictable or the time-predictable behaviour at a given point on the fault (Fig. 2d). The model does not exhibit the time-predictable behaviour because the model does not incorporate a fixed threshold shear stress for slip to occur. The behaviour is closer to being slip predictable, even more so if the average slip (or equivalently the slip potency) is considered rather than slip at one particular point (Fig. 2e). This is because, after each earthquake, the shear stress on the ruptured area drops to the same level, approximately determined by the steady-state friction equation (1) evaluated at the coseismic slip rate $V = V_{dyn}$ ($\sim$1–10 m s^{-1}). The simulations also show that assessing whether the fault exhibits time- or slip-predictable behaviour requires an extended history with many earthquake cycles.

Quantifying the effect of VS patches on seismic ruptures

The effect of the central VS patch on the resulting pattern of large earthquakes can be quantified in terms of the probability that an earthquake that has ruptured one VW segment would propagate through the VS patch, rupturing at least a part of the second VW segment. The probability is estimated from the percentage P of earthquakes that propagate through the VS patch relative to the number of earthquakes that rupture entirely one of the two VW segments.

Clearly, the larger the length D_{vs} of the VS patch and the higher the average stress increase $\Delta\tau_{prop}$ required for seismic slip within the VS patch, the smaller would be the percentage of earthquakes that propagate through the VS patch. An approximation for $\Delta\tau_{prop}$ can be obtained by considering the difference in average shear stress on the patch before and during seismic slip and a further contribution from the breakdown work[46], a quantity sometimes called fracture energy. Hence we define the resistance C of the VS patch as (Supplementary Information S3)

$$C = \Delta\tau_{prop}D_{vs} = \bar{\sigma}_{vs}(a_{vs} - (1-\lambda^*)b_{vs})\ln\left(V_{dyn}/V_i\right)D_{vs} \qquad (2)$$

where the subscript 'vs' refers to the parameters characterizing the VS patch, $0 \leq \lambda^* \leq 1$ accounts for breakdown work at the crack tip, and V_{dyn} and V_i are the representative seismic slip velocity and slip velocity at the end of the interseismic period on the VS patch. The values of V_{dyn} and V_i depend on the model behaviour, but their variation is limited in our simulations. V_{dyn} is of the order of the typical seismic slip velocity of $1\,m\,s^{-1}$, and V_i ranges from the plate velocity of $10^{-9}\,m\,s^{-1}$ to values smaller by 1–2 orders of magnitude, so that $\ln(V_{dyn}/V_i) \approx 20$, nearly independent of the model parameters. Inclusion of parameter λ^* is only important for patches with friction properties close to velocity neutral (Supplementary Information S3). Hence, for most cases, the patch resistance (equation (2)) can be approximated by $C_{appr} = 20\bar{\sigma}_{vs}(a_{vs} - b_{vs})D_{vs}$.

This is exactly what our simulations show (Fig. 4a). In simulations with a broad range of patch parameters D_{vs} and $\bar{\sigma}_{vs}(a_{vs} - b_{vs})$, the percentage P of two-segment ruptures is approximately constant for the same value of C_{appr} (Fig. 4a). Smaller values of C_{appr} enable nearly every rupture to propagate through the VS patch, larger values result in the patch acting as a permanent barrier and intermediate values allow for a rich behaviour with comparable numbers of earthquakes arresting and propagating through the patch as in the case of Fig. 2.

The properties of VW segments also significantly affect probability P. Rupture of a VW segment increases stress on the VS patch, and the larger the stress increase, the larger P is expected to become. The stress increase can be represented (Supplementary Information S3) as $\beta\Delta\tau_{vw}D_{vw}$, where $\Delta\tau_{vw}$ is the average stress drop over the VW segment, D_{vw} is the length of the VW segment and β is a model-dependent geometric factor between 0 and 1. For the 3D model, both the patch resistance and the transferred stress need to be multiplied by the seismogenic fault width W. We use $\beta = 1/2$ for the 2D model and $\beta = W/(2D_{vw} + 2W)$ for the 3D model. This is based on the assumption that stress is transferred equally in all directions and that, in 3D models, β is proportional to the perimeter of the VW segment that is contiguous with the VS patch.
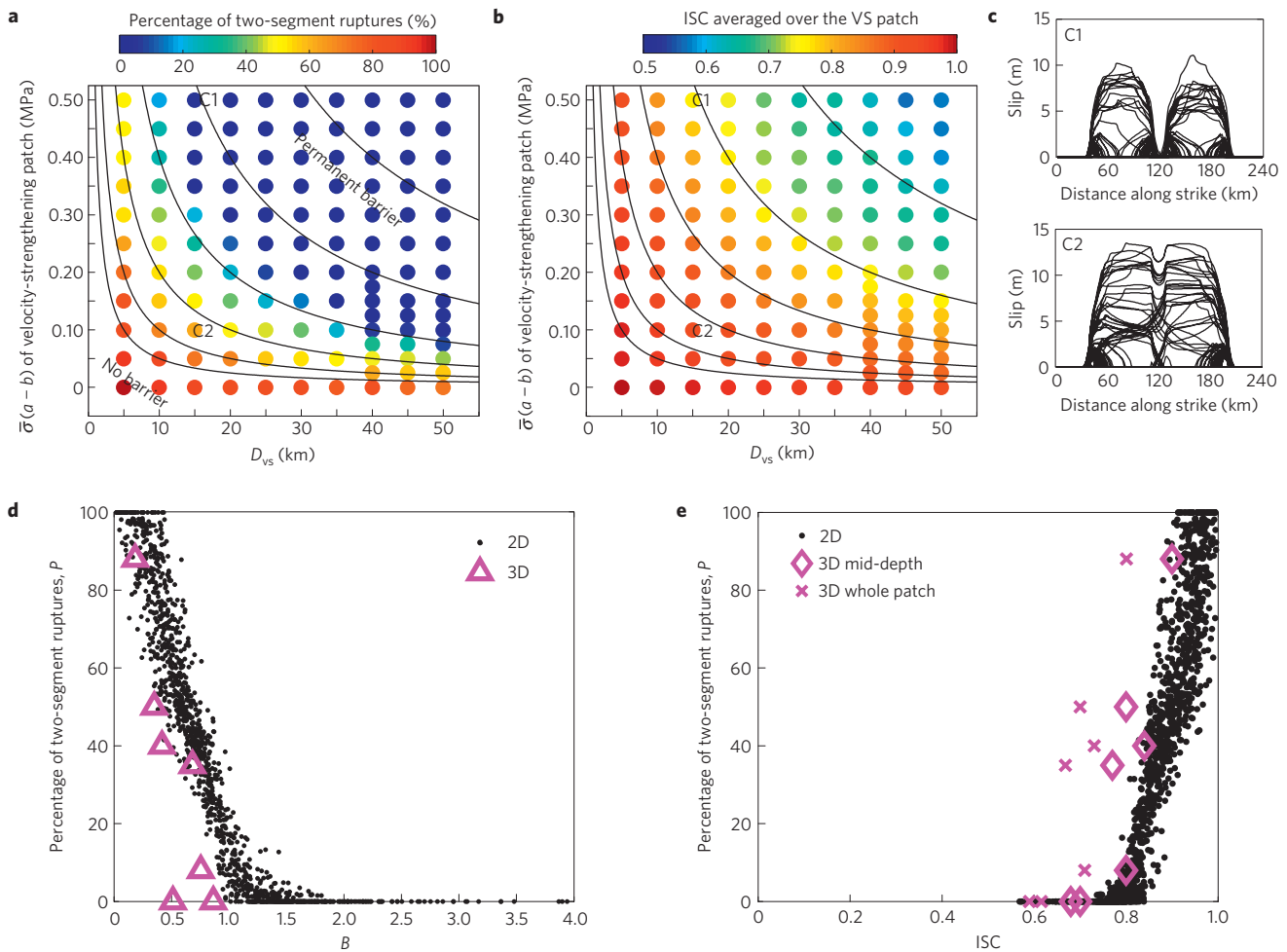
Figure 4 | Relation between the properties of VS and VW regions, probability _P_ that an earthquake would propagate through the VS patch, and ISC.
a,b, Properties of the VS patch have a similar systematic effect on both the pattern of seismic ruptures, as quantified by _P_, and ISC averaged over the patch.
_P_ = 0% corresponds to a permanent barrier. Each colour of dot represents a 2D simulation of 9000 yr of fault slip, with more than 50 events that rupture
either one or both VW segments. Isocontours of $\bar{\sigma}(a_{vs} - b_{vs})D_{vs}$ (solid lines) pass through similar values of _P_ and ISC in **a** and **b**, respectively. Properties of
the VW segments are the same for all cases. **c**, Slip distributions of events corresponding to cases C1 and C2 illustrate the range of model behaviour. The
VS patch can either act as a permanent barrier (C1) or enable most of the earthquakes to propagate through (C2), despite being of the same size.
d, Relation between _P_ and non-dimensional parameter _B_ for several 3D simulations and a large set of 2D simulations in which the properties of both VW
and VS regions are systematically varied (Supplementary Table S1). All results collapse, with some scatter, onto a single curve. **e**, The percentage _P_ of
two-segment ruptures and ISC averaged over the VS patch are closely related. The labels '3D mid-depth' and '3D whole patch' correspond to ISC averaged
over the mid-seismogenic depth and over the entire VS patch, respectively.

The barrier efficiency of a VS patch can thus be characterized
with the non-dimensional parameter:

$$B = \frac{\Delta\tau_{prop}D_{vs}}{\beta\,\Delta\tau_{vw}D_{vw}} \tag{3}$$

which can be approximated by $B_{appr} = (20\bar{\sigma}_{vs}(a_{vs} - b_{vs})D_{vs})/$
$(\beta\Delta\tau_{vw}D_{vw})$ for most cases. The larger the _B_ value, the smaller
should be the percentage of ruptures that propagate through
the patch. Figure 4d shows that _P_ is indeed correlated with _B_
(equation (3)) for a large number of simulations in which we have
varied the properties and sizes of the VW and VS segments, and
the effective normal stress (Supplementary Table S1). This plot
demonstrates that _B_ is an appropriate parameter to quantify the
effect of the VS patch on the pattern of large earthquakes. The
results of 2D and 3D models collapse nearly onto the same curve in Fig. 4d,
showing that parameter _B_ can be used to connect the results of the
2D model to the more realistic 3D situations. This also means that,
for the same characteristics of the VW and VS regions that enter

_B_, the VS patch acts as a stronger barrier in the 3D model, because
the value of β is smaller for the 3D model (1/6 for the particular
geometry used, with $W = D_{vw}/2$).

Relation of ISC to rupture patterns and individual events
Our simulations indicate that the size and friction properties of
the VS patch influence ISC similarly to the effect on earthquake
ruptures (Fig. 4). ISC decreases as either D_{vs} or $\bar{\sigma}_{vs}(a_{vs} - b_{vs})$
increases, with the ISC being approximately the same for a constant
value of their product C_{appr} (Fig. 4b). For a wide range of model
parameters, we find that ISC in the VS patch correlates with the
percentage _P_ of earthquakes rupturing through it (Fig. 4e). This has
an important implication for seismic hazard because the rupture
extent of large earthquakes is linked to variations in ISC. This
conclusion holds for both 2D and 3D simulations. Note that, for
the same percentage _P_ of two-segment ruptures, ISC is lower in
the 3D simulations, because there the VS patch is directly loaded
by the adjacent larger VS regions that creep at nearly the plate
loading rate. Regardless of the model or how the values of ISC

are computed, a VS patch with a locally lower, but still high, ISC (ISC $\lesssim 0.6$) can systematically arrest coseismic ruptures (Fig. 4e). This means that a VS patch compensates for the deficit in seismic slip not through a significant decrease in ISC, but rather through significant postseismic slip after events that stop near the patch.

The correlation between ISC and earthquake patterns characterized by P is not surprising. Accumulated slip must be relatively uniform over the fault domain and equal to the sum of co-, post- and interseismic slip. It follows that the overall seismic behaviour of the VS patch is related to the amount of cumulative slip occurring in the interseismic period, and hence to ISC. The correlation between ISC and P implies that ISC also depends on the non-dimensional parameter B. In fact, it can be shown that ISC and B_{appr} are related in a spring–slider model for cases when the patch acts as a permanent barrier (Supplementary Information S4).

We observe that the source-time function of earthquakes that rupture through a VS patch contains multiple peaks (Fig. 2g), the phenomenon commonly inferred from inversions of large earthquakes[6,43,44]. This is because both the potency rate and rupture speed first decrease as rupture propagates through the central VS patch and then increase after the rupture front enters the neighbouring VW segment. However, a multiple-peaked source-time function could also arise owing to a region of lower prestress on a VW fault (sometimes referred to as an 'anti-asperity'). The two types of heterogeneity can be distinguished from postseismic observations, because afterslip would occur within a VS patch (Fig. 2f) but not within a VW region of lower prestress. Thus, variations in seismic potency rates combined with the distribution of postseismic slip can be used to infer smaller-scale heterogeneities in friction properties within a locked region of high but variable ISC.

Towards quantitative seismic hazard assessment

This study demonstrates that friction heterogeneities provide a unifying explanation for a variety of observations of fault behaviour regarding individual ruptures, earthquake sequences and patterns of ISC. Fault areas with VS friction, which can be detected from geodetic or remote-sensing measurements of interseismic and postseismic strain, may be the primary cause for the relative persistence of seismic rupture segmentation and asperities. At the same time, the presence of such VS patches can explain other aspects of the long-term seismic behaviour of faults such as clustering of large events, overlapping of subsequent ruptures and ruptures of several locked segments. Our results suggest that relatively small VS patches could have a profound effect on the long-term seismic behaviour but a subtle effect on ISC.

The presented work provides physical insights into how spatial heterogeneities in fault friction properties—observed through seismic, postseismic and interseismic slip—can influence future earthquakes. Thus, our study opens up ways to make quantitative use of geodetic and seismic observations for seismic-hazard assessment. This study focuses on large earthquakes on subduction megathrusts. However, our conclusions should be applicable to any environment and scale, including smaller scales, that contain heterogeneities in fault friction properties.

References

1. Shimazaki, K. & Nakata, T. Time-predictable recurrence model for large earthquakes. *Geophys. Res. Lett.* **7**, 279–282 (1980).
2. Schwartz, D. P. & Coppersmith, K. J. Fault behaviour and characteristic earthquakes: Examples from the Wasatch and San Andreas fault zones. *J. Geophys. Res.* **89**, 5681–5698 (1984).
3. Schwartz, S. Y. Noncharacteristic behavior and complex recurrence of large subduction zone earthquakes. *J. Geophys. Res.* **104**, 23111–23125 (1999).
4. Murray, J. & Segall, P. Testing time-predictable earthquake recurrence by direct measurement of strain accumulation and release. *Nature* **419**, 287–291 (2002).
5. Weldon, R., Fumal, T. & Biasi, G. Wrightwood and the earthquake cycle: What a long recurrence record tells us about how faults works. *GSA Today* **14**, 4–10 (2004).
6. Konca, O. A. *et al.* Partial rupture of a locked patch of the Sumatra megathrust during the 2007 earthquake sequence. *Nature* **456**, 631–635 (2008).
7. Thatcher, W. Order and diversity in the modes of Circum-Pacific earthquake recurrence. *J. Geophys. Res.* **91**, 2609–2623 (1990).
8. Sieh, K. *et al.* Earthquake supercycles inferred from sea-level changes recorded in the corals of west Sumatra. *Science* **322**, 1674–1678 (2008).
9. Kanamori, H. & McNally, K. C. Variable rupture mode of the subduction zone along the Ecuador–Colombia coast. *Bull. Seismol. Soc. Am.* **72**, 1241–1253 (1982).
10. Rundle, J. B., Kanamori, H. & McNally, K. C. An inhomogeneous fault model for gaps, asperities, barriers and seismicity migration. *J. Geophys. Res.* **89**, 10219–10231 (1987).
11. Cochard, A. & Madariaga, R. Complexity of seismicity due to highly rate-dependent friction. *J. Geophys. Res.* **101**, 25321–25336 (1996).
12. Ariyoshi, K. *et al.* Character of slip and stress due to interaction between fault segments along the dip direction of a subduction zone. *J. Geodyn.* **48**, 55–67 (2009).
13. Wesnousky, S. G. Predicting the endpoints of earthquake ruptures. *Nature* **444**, 358–360 (2006).
14. Freymueller, J. T., Cohen, S. C. & Fletcher, H. J. Spatial variations in present-day deformation, Kenai Peninsula, Alaska, and their implications. *J. Geophys. Res.* **105**, 8079–8101 (2000).
15. Igarashi, T., Matsuzawa, T. & Hasegawa, A. Repeating earthquakes and interplate aseismic slip in the northeastern Japan subduction zone. *J. Geophys. Res.* **108**, 2249 (2003).
16. Chlieh, M., Avouac, J-P., Sieh, K., Natawidjaja, D. H. & Galetzka, J. Heterogeneous coupling of the Sumatran megathrust constrained by geodetic and paleogeodetic measurements. *J. Geophys. Res.* **113**, B05305 (2008).
17. Moreno, M. S., Klotz, J., Melnick, D., Echtler, H. & Bataille, K. Active faulting and heterogeneous deformation across a megathrust segment boundary from GPS data, south central Chile (36°–39° S). *Geochem. Geophys. Geosyst.* **9**, Q12024 (2008).
18. Hashimoto, C., Noda, A., Sagiya, T. & Matsu'ura, M. Interplate seismogenic zones along the Kuril–Japan trench inferred from GPS data inversion. *Nature Geosci.* **2**, 141–144 (2009).
19. Perfettini, H. *et al.* Aseismic and seismic slip on the megathrust offshore southern Peru revealed by geodetic strain. *Nature* (in the press).
20. Yamanaka, Y. & Kikuchi, M. Asperity map along the subduction zone in northeastern Japan inferred from regional seismic data. *J. Geophys. Res.* **109**, B07307 (2004).
21. Ito, T., Yoshioka, S. & Miyazaki, S. Interplate coupling in northeast Japan deduced from inversion analysis of GPS data. *Earth Planet. Sci. Lett.* **176**, 117–130 (2000).
22. Hsu, Y-J. *et al.* Frictional afterslip following the 2005 Nias–Simeulue earthquake, Sumatra. *Science* **312**, 1921–1926 (2006).
23. Miyazaki, S., Segall, P., Fukuda, J. & Kato, T. Space time distribution of afterslip following the 2003 Tokachi-oki earthquake: Implications for variations in fault zone frictional properties. *Geophys. Res. Lett.* **31**, L06623 (2004).
24. Baba, T., Hirata, K., Hori, T. & Sakaguchi, H. Offshore geodetic data conducive to the estimation of the afterslip distribution following the 2003 Tokachi-oki earthquake. *Earth Planet. Sci. Lett.* **241**, 281–292 (2006).
25. Johanson, I. A., Fielding, E. J., Rolandone, F. & Bürgmann, R. Coseismic and postseismic slip of the 2004 Parkfield earthquake from space-geodetic data. *Bull. Seismol. Soc. Am.* **96**, 269–282 (2006).
26. Rubin, A. M., Gillard, D. & Got, J-L. Streaks of microearthquakes along creeping faults. *Nature* **400**, 635–641 (1999).
27. Bourouis, S. & Bernard, P. Evidence for coupled seismic and aseismic fault slip during water injection in the geothermal site of Soultz (France), and implications for seismogenic transients. *Geophys. J. Int.* **169**, 723–732 (2007).
28. Dieterich, J. H. Time-dependent friction and the mechanics of stick–slip. *J. Geophys. Res.* **116**, 790–806 (1978).
29. Ruina, A. L. Slip instability and state variable friction laws. *J. Geophys. Res.* **88**, 10359–10370 (1983).
30. Blanpied, M. L., Lockner, D. A. & Byerlee, J. D. Frictional slip of granite at hydrothermal conditions. *J. Geophys. Res.* **100**, 13045–13064 (1995).
31. Marone, C. Laboratory-derived friction laws and their application to seismic faulting. *Annu. Rev. Earth Planet. Sci.* **26**, 643–696 (1998).
32. Dieterich, J. H. Applications of rate- and state-dependent friction to models of fault slip and earthquake occurrence. *Treat. Geophys.* **4**, 107–129 (2007).
33. Tse, S. & Rice, J. R. Crustal earthquake instability in relation to the depth variation of frictional slip properties. *J. Geophys. Res.* **91**, 9452–9472 (1986).

34. Rice, J. R. & Ruina, A. L. Stability of steady frictional slipping. *J. Appl. Mech.* **50,** 343–349 (1983).

35. Ben-Zion, Y. & Rice, J. R. Slip patterns and earthquake populations along different classes of faults in elastic solids. *J. Geophys. Res.* **100,** 12959–12983 (1995).

36. Tullis, T. E. Rock friction and its implications for earthquake prediction examined via models of Parkfield earthquakes. *Proc. Natl Acad. Sci. USA.* **93,** 3803–3810 (1996).

37. Lapusta, N., Rice, J., Ben-Zion, Y. & Zheng, G. Elastodynamic analysis for slow tectonic loading with spontaneous rupture episodes on faults with rate- and state-dependent friction. *J. Geophys. Res.* **105,** 23765–23789 (2000).

38. Hori, T., Kato, N., Hirahara, K., Baba, T. & Kaneda, Y. A numerical simulation of earthquake cycles along the Nankai trough, southwest Japan: Lateral variation in frictional property due to slab geometry controls the nucleation position. *Earth Planet. Sci. Lett.* **228,** 215–226 (2004).

39. Rice, J. R. Spatio-temporal complexity of slip on a fault. *J. Geophys. Res.* **98,** 9885–9907 (1993).

40. Boatwright, J. & Cocco, M. Frictional constraints on crustal faulting. *J. Geophys. Res.* **101,** 13895–13909 (1996).

41. Chen, T. & Lapusta, N. Scaling of small repeating earthquakes explained by interaction of seismic and aseismic slip in a rate and state fault model. *J. Geophys. Res.* **114,** B01311 (2009).

42. Suito, H. & Freymueller, J. T. A viscoelastic and afterslip postseismic deformation model for the 1964 Alaska earthquake. *J. Geophys. Res.* **114,** B11404 (2009).

43. Christensen, D. H. & Beck, S. L. The rupture process and tectonic implications of the great 1964 Prince William sound earthquake. *Pure Appl. Geophys.* **142,** 29–53 (1994).

44. Sladen, A. *et al.* Source model of the 2007 M_w 8.0 Pisco, Peru earthquake—implications for seismogenic behavior of subduction megathrusts. *J. Geophys. Res.* **115,** B02405 (2010).

45. Lapusta, N. & Liu, Y. Three-dimensional boundary integral modeling of spontaneous earthquake sequences and aseismic slip. *J. Geophys. Res.* **114,** B09303 (2009).

46. Tinti, E., Spudich, P. & Cocco, M. Earthquake fracture energy inferred from kinematic rupture models on extended faults. *J. Geophys. Res.* **110,** B12303 (2005).

Author contributions

Y.K. designed the study, carried out and analysed the numerical experiments and wrote the paper. J-P.A. and N.L. analysed the numerical experiments and contributed to the concept development. All authors discussed the results and commented on the paper.

Additional information

The authors declare no competing financial interests. Supplementary information accompanies this paper on www.nature.com/naturegeoscience. Reprints and permissions information is available online at http://npg.nature.com/reprintsandpermissions. Correspondence and requests for materials should be addressed to Y.K.

Towards inferring earthquake patterns from geodetic observations of interseismic coupling

Nature Geoscience 2010

Yoshihiro Kaneko, Jean-Philippe Avouac, Nadia Lapusta

March 17, 2010

List of Tables

List of Figures

S1   Computation of Interseismic Coupling (ISC)

Interseismic coupling (ISC) is defined as the ratio of slip deficit during the interseismic period divided by the long term slip that would have happened if the fault had been slipping at it long term average slip rate. In our model, ISC at any location x on the fault is computed from $\text{ISC}(x) = 1 - \delta_{\text{int}}^{\text{cum}}(x)/[V_{\text{pl}}T_{\text{int}}^{\text{cum}}(x)]$, where $T_{\text{int}}^{\text{cum}}$ is sum of the interseismic time intervals at the location x for the entire simulation and $\delta_{\text{int}}^{\text{cum}}$ is the slip accumulated at x over all interseismic periods. The interseismic periods $T_{\text{int}}(x)$ are defined to be the time when slip rate $V(x,t)$ is less than the long-term slip rate V_{pl}.

S2   Description of the fault models and parameters

We use fault models (*Lapusta et al.*, 2000; *Lapusta and Liu*, 2009) in which earthquakes are simulated as a part of spontaneously occurring earthquake sequences on a fault that is subjected to slow, tectonic-like loading. This approach allows us to study naturally developing earthquakes, with conditions before the nucleation originating from the previous history of fault slip rather than from arbitrarily selected prestress. Our simulations resolve all stages of the seismic cycle: the aseismic nucleation process in gradually varying zones of accelerating slip, the subsequent inertially controlled event (unstable slip) with realistic slip rates and rupture speeds, the postseismic slip, and the interseismic quasi-static deformation between events.

The fault is governed by rate and state friction with the aging form of state variable evolution. For situations with time-independent effective normal stress $\bar{\sigma}$, the shear strength τ is expressed as

$$\tau = \bar{\sigma}\left[f_0 + a\ln\left(\frac{V}{V_0}\right) + b\ln\left(\frac{V_0\theta}{L}\right)\right] , \tag{S1}$$

$$\frac{d\theta}{dt} = 1 - \frac{V\theta}{L} , \tag{S2}$$

where a and b are rate and state constitutive parameters, V is slip rate, f_0 is the reference friction coefficient corresponding to the reference slip rate V_0, θ is a state variable which can be interpreted as the average age of the population of contacts between two surfaces, and L is the characteristic slip for state evolution (*Dieterich*, 1978, 1979; *Ruina*, 1983). The actual fault resistance to sliding in our model is given by rate and state friction regularized at zero slip velocity (*Lapusta et al.*, 2000). The response of constitutive laws (Eq. S1-S2), when extrapolated to coseismic slip rates, becomes qualitatively similar to the one given by linear slip-weakening friction (*Cocco and Bizzarri*, 2002) commonly used in dynamic rupture models (*Day et al.*, 2005).

We use parameters applicable to natural faults or derived from laboratory experiments except for characteristic slip L. The typical value of L used is 8 mm, larger than the laboratory values of the order of 1-100 μm, to make the breakdown work (sometimes called seismological fracture energy) comparable to values inferred from observational studies. For instance, the estimated breakdown work in the example in Fig. 2 is 2 MJ/m^2, which falls in the range of the breakdown work inferred for M>7 earthquakes (*Abercrombie and Rice*, 2005). Unless stated otherwise, we use the following set of parameters: $\mu = 30$ GPa, $c_s = 3.3$ km/s, $\bar{\sigma} = 50$ MPa, $f_0 = 0.6$, $V_0 = 10^{-6}$

m/s, $a_{vw} = 0.010$, $b_{vw} = 0.015$, and the size of the VW segment $D_{vw} = 72.5$ km, where the subscript 'vw' is used to denote quantities related to the VW segments.

S2.1   Two-dimensional (2D) fault model

The 2D fault model is based on an antiplane (Mode III) framework in which purely dip-slip motion is assumed. Only along-strike (parallel to the x axis) variations are considered. The relation between slip $\delta(x,t)$, slip velocity $V(x,t) = \partial\delta(x,t)/\partial t$, and the corresponding shear stress $\tau(x,t)$ is given by (*Rice*, 1993; *Lapusta et al.*, 2000)

$$\tau(x,t) \; = \; \tau^o(x) + f(x,t) - \frac{\mu}{2c_s}V(x,t) \;, \tag{S3}$$

where μ is the shear modulus, c_s is the shear wave speed, τ^o is the loading stress that would act on the interface if it were constrained against any slip, and $f(x,t)$ is a linear functional of prior slip over the causality cone. The last term, known as radiation damping, is extracted from the functional $f(x,t)$ so that $f(x,t)$ can be evaluated without concern for singularities. The details of the elastodynamic solution and simulation methodology can be found elsewhere (*Lapusta et al.*, 2000).

The simulated fault domain is 480 km long. Slip evolution is computed, based on the assumed friction law, on the 240-km long central portion, and the prescribed slip rate $V_{pl} = 5$ cm/year is imposed on the two 120-km long outer portions of the model (Fig. 1b). The spatial cell size Δx needs to be small enough to properly resolve both the aseismic nucleation process and the cohesive zone size during dynamic rupture propagation. In all of our simulations, the proper resolution of the cohesive-zone imposes a more stringent constraint on the spatial discretization. The ratio $\Lambda/\Delta x$ of the cohesive zone size Λ to the cell size $\Delta x = 29$ m needs to be 3 or larger for faults with rate and state friction (*Kaneko et al.*, 2008). The value of Λ in a typical scenario is ≈ 0.3 km and hence $\Lambda/\Delta x > 3$ in our simulations. The resulting ratio $h^*_{RA}/\Delta x = 2\mu bL/[\pi(b-a)^2\bar{\sigma}\Delta x] = 63$, where h^*_{RA} is the estimate of the nucleation size for $a/b \gtrsim 0.5$ (*Rubin and Ampuero*, 2005), is then high enough to properly resolve the nucleation processes.

Time t is discretized into variable time steps. The minimum value of the time step is related to the time $\Delta t_{cell} = \Delta x/c_s$ needed for the shear wave to propagate through one spatial cell; it is given by $0.5\Delta x/c_s = 0.044$ s. Such a small value of Δt_{min} is needed because slip in one time step must be comparable to or smaller than the characteristic slip L of the friction law to resolve the state-variable evolution. The largest time step allowed in all simulations is 0.2 years. A typical simulation with 5000 years of simulated slip history takes 5 days on a single 2.33-GHz core.

S2.2   Three-dimensional (3D) fault model

The 3D model formulation (*Lapusta and Liu*, 2009) is an extension of the 2D one. The major difference is that the 3D fault model allows for variations in the along-dip direction (Fig. 1c). The relation between slip $\delta_i(x,z,t)$, slip velocity $V_i(x,z,t)$, and the corresponding shear stress $\tau_{yi}(x,z,t) = \tau_i(x,z,t)$, $i = x,y,z$ on the fault plane $y = 0$ is expressed as

$$\tau_i(x,z;t) \; = \; \tau_i^o(x,z) + f_i(x,z;t) - \eta_i V_i(x,z;t) \;, \tag{S4}$$

where $\eta_x = \eta_z = \mu/(2c_s)$, $\eta_y = \mu c_p/(2c_s^2)$ and c_p is the dilatational wave speed. The details of the elastodynamic solution and simulation methodology for the model can be found elsewhere (*Lapusta and Liu*, 2009).

To facilitate comparison between the 2D and 3D simulations, we use the same set of parameters except for two parameters that are only defined in the 3D model: the dilatational wave speed c_p and the seismogenic width W (Fig. 1c). We assign $c_p = \sqrt{3}c_s$ and $W = D_{vw}/2 = 36.25$ km. The effective normal stress $\bar{\sigma}(z)$ linearly increases in the down-dip direction, from 30 MPa at the top of the simulated region to 70 MPa at the bottom of it, with $\bar{\sigma}(z) = 50$ MPa along a horizontal line at the mid-depth of the seismogenic zone.

The simulated fault domain is 300 km long along strike and 150 km wide along dip. The along strike-variations are the same as in the 2D models. In the along-dip direction, we consider a 75-km wide region, where slip is determined by solving the elastodynamic equations based on the assumed friction law, and two 37.5-km wide loading regions with prescribed slip rate (Fig. 1c). The cell size is $\Delta x = \Delta z = 0.14$ km, and the cohesive zone size Λ in a 3D simulation is ≈ 0.3 km. Hence, $\Lambda/\Delta x \approx 2.2$, which gives marginal but acceptable discretization (*Day et al.*, 2005; *Kaneko et al.*, 2008). Since a 3D simulation is much more computationally expensive than a 2D one, we performed a total of seven 3D simulations with different values of parameters $\bar{\sigma}_{vs}(a_{vs} - b_{vs})$ or D_{vs} (Fig. 4c,d). With the geometry and spatial discretization adopted here, a 3D simulation for an earthquake sequence that produces 30-40 events takes one week with 250 cores on a supercomputer.

S3   Construction of the non-dimensional model parameter B

To construct parameter B that determines the probability that seismic rupture would propagate through the VS patch, we consider the ratio of the following two quantities: (i) stress increase required for the patch to sustain seismic slip, and (ii) stress transferred from the ruptured VW segment to the VS patch.

Let us first consider the stress increase required for the VS patch to sustain seismic slip integrated over the patch, $C = \Delta\tau_{prop}D_{vs}$, where $\Delta\tau_{prop}$ is the average required amount of shear stress increase and D_{vs} is the size of the VS patch. We refer to C as the VS patch resistance. To estimate $\Delta\tau_{prop}$, let us first consider the difference in shear stress on the VS patch before and during seismic slip. Prior to the arrival of seismic rupture, the shear stress on the VS patch is given by:

$$\tau_{vs}^i = \bar{\sigma}_{vs}\left[f_0 + (a_{vs} - b_{vs})\ln\left(V_{vs}^i/V_0\right)\right] \; , \tag{S5}$$

where V_{vs}^i is the representative interseismic slip rate in the VS patch. During seismic slip with slip rate V_{vs}^{dyn}, shear stress in the patch can be approximated as

$$\tau_{vs}^d = \bar{\sigma}_{vs}\left[f_0 + (a_{vs} - b_{vs})\ln\left(V_{vs}^{dyn}/V_0\right)\right] \; . \tag{S6}$$

Hence

$$\Delta\tau_{\mathrm{prop}} = \tau_{\mathrm{vs}}^{\mathrm{d}} - \tau_{\mathrm{vs}}^{\mathrm{i}} = \bar{\sigma}_{\mathrm{vs}}(a_{\mathrm{vs}} - b_{\mathrm{vs}}) \ln\left(V_{\mathrm{vs}}^{\mathrm{dyn}}/V_{\mathrm{vs}}^{\mathrm{i}}\right) \ . \tag{S7}$$

This analysis ignores the larger but shorter-lived stress increase at the rupture tip, which becomes progressively more important as $(a_{\mathrm{vs}} - b_{\mathrm{vs}})$ approaches zero; a velocity-neutral patch would still provide resistance to the rupture propagation through the breakdown work at the rupture tip. This effect can actually be incorporated. At the onset of seismic slip with slip rate $V_{\mathrm{vs}}^{\mathrm{dyn}}$, the shear stress in the VS patch abruptly increases to a peak value approximately given by

$$\tau_{\mathrm{vs}}^{\mathrm{p}} = \bar{\sigma}_{\mathrm{vs}} \left[f_0 + a_{\mathrm{vs}} \ln\left(V_{\mathrm{vs}}^{\mathrm{dyn}}/V_0\right) + b_{\mathrm{vs}} \ln\left(V_0/V_{\mathrm{vs}}^{\mathrm{i}}\right) \right] \ , \tag{S8}$$

and drops to the value $\tau_{\mathrm{vs}}^{\mathrm{d}}$ given by Eq. (S6) over the effective weakening distance $d_{\mathrm{vs}}^{\mathrm{c}}$ (Fig. S1). The resulting breakdown work density is given by $(\tau_{\mathrm{vs}}^{\mathrm{p}} - \tau_{\mathrm{vs}}^{\mathrm{d}})d_{\mathrm{vs}}^{\mathrm{c}}/2$, and this part of work is additional to the friction work density $(\tau_{\mathrm{vs}}^{\mathrm{d}} - \tau_{\mathrm{vs}}^{\mathrm{i}})\delta_{\mathrm{vs}}$ that arises due to stress increase (Eq. S7), where δ_{vs} is the amount of seismic slip averaged over the patch. Hence to account for the transient stress increase at the rupture tip, we write

$$\Delta\tau_{\mathrm{prop}} = \frac{d_{\mathrm{vs}}^{\mathrm{c}}}{2\delta_{\mathrm{vs}}}(\tau_{\mathrm{vs}}^{\mathrm{p}} - \tau_{\mathrm{vs}}^{\mathrm{d}}) + (\tau_{\mathrm{vs}}^{\mathrm{d}} - \tau_{\mathrm{vs}}^{\mathrm{i}}) \tag{S9}$$

$$= \bar{\sigma}_{\mathrm{vs}}(a_{\mathrm{vs}} - \lambda^* b_{\mathrm{vs}}) \ln\left(V_{\mathrm{vs}}^{\mathrm{dyn}}/V_{\mathrm{vs}}^{\mathrm{i}}\right) \ , \tag{S10}$$

where

$$\lambda^* \equiv 1 - d_{\mathrm{vs}}^{\mathrm{c}}/(2\delta_{\mathrm{vs}}) \ . \tag{S11}$$

The patch resistance to seismic slip can therefore be written as:

$$C = \Delta\tau_{\mathrm{prop}}D_{\mathrm{vs}} = \bar{\sigma}_{\mathrm{vs}}(a_{\mathrm{vs}} - \lambda^* b_{\mathrm{vs}})D_{\mathrm{vs}} \ln\left(V_{\mathrm{vs}}^{\mathrm{dyn}}/V_{\mathrm{vs}}^{\mathrm{i}}\right) \ . \tag{S12}$$

The first term on the right-hand side of Eq. (S9) corresponds to the contribution from the transient stress increase at the crack tip, and, in most cases we have considered, it amounts to a few percent of the second term. Let us estimate λ^*. For the rate and state friction with the aging form of state variable evolution, the effective weakening distance is given by (*Cocco and Bizzarri*, 2002; *Rubin and Ampuero*, 2005) $d_{\mathrm{vs}}^{\mathrm{c}} = L_{\mathrm{vs}} \ln(V_{\mathrm{vs}}^{\mathrm{dyn}}/V_{\mathrm{vs}}^{\mathrm{i}})$, where $\ln(V_{\mathrm{vs}}^{\mathrm{dyn}}/V_{\mathrm{vs}}^{\mathrm{i}}) \approx 20$ in our simulations, nearly independently of the properties of the VS patch as discussed in the main text. δ_{vs} can be estimated as a fraction (we use 1/2) of the maximum slip in the nearby velocity-weakening segment. If $\Delta\tau_{\mathrm{vw}}$ is the average stress drop over the VW segment, D_{vw} is the size of the VW segment, and rupture over the VW segment is approximated as a quasi-static crack, then we have $\delta_{\mathrm{vs}} = \Delta\tau_{\mathrm{vw}}D_{\mathrm{vw}}/(2\mu)$. Hence we get

$$\lambda^* = 1 - \frac{\mu L_{\mathrm{vs}} \ln(V_{\mathrm{dyn}}/V_{\mathrm{i}})}{\Delta\tau_{\mathrm{vw}}D_{\mathrm{vw}}} \ . \tag{S13}$$

For the typical values of the model parameters, both assigned ($\mu = 30$ GPa, $L_{\mathrm{vs}} = 8$ mm, $D_{\mathrm{vw}} = 72.5$ km) and resulting in the model ($\Delta\tau_{\mathrm{vw}} = 3$ MPa, $\ln(V_{\mathrm{vs}}^{\mathrm{dyn}}/V_{\mathrm{vs}}^{\mathrm{i}}) \approx 20$), we obtain

$\lambda^* = 0.98$. This is why the effect represented by λ^* can be ignored for patches that are not close to velocity-neutral, with the patch resistance C approximately given by C_{appr} defined in the main text. Note that the smaller the characteristic slip L_{vs} of the rate and state friction, the closer the value of λ^* to one.

Now let us consider the stress transferred to the VS patch by rupture of a VW segment. We start from the 2D elastodynamic equation (Eq. S3), where shear stress distribution $\tau(x)$ during a seismic event can be written as

$$\tau(x) \; = \; \tau^{\mathrm{before}}(x) + f(x,t) - \frac{\mu}{2c_s}V(x) \; , \tag{S14}$$

where $\tau^{\mathrm{before}}(x)$ is shear stress before the event and $f(x,t)$ is redefined accordingly. Integrating Eq. (S14) over the entire fault after the rupture of a single VW segment, we obtain

$$\int_x \tau(x)dx \; = \; \int_x \tau^{\mathrm{before}}(x)dx - \frac{\mu}{2c_s}\int_x V(x)dx \; , \tag{S15}$$

since the integral over $f(x,t)$ is zero (*Zheng and Rice*, 1998). The last term on the right-hand side is negligible compared to others, since slip velocity after the end of a seismic event is small ($V \lesssim 1$ mm/s). Ignoring that term, we obtain

$$\int_x \left[\tau(x) - \tau^{\mathrm{before}}(x)\right] dx = 0 \; , \tag{S16}$$

or

$$\int_{\mathrm{vw}} \left[\tau(x) - \tau^{\mathrm{before}}(x)\right] dx + \int_{\mathrm{vs}} \left[\tau(x) - \tau^{\mathrm{before}}(x)\right] dx = 0 \; . \tag{S17}$$

Considering the situation where one of the VW segments has ruptured and transferred stress onto the surrounding VS regions, we get

$$\int_0^{D_{\mathrm{vw}}} \Delta\tau_{\mathrm{vw}}(x)dx \equiv \Delta\tau_{\mathrm{vw}}D_{\mathrm{vw}} = \int_{\mathrm{VS\ patch}} \Delta\tau_{\mathrm{vs}}(x)dx + \int_{\mathrm{VS\ other}} \Delta\tau_{\mathrm{vs}}(x)dx \; , \tag{S18}$$

where $\Delta\tau_{\mathrm{vw}}(x)$ and $\Delta\tau_{\mathrm{vw}}$ are the coseismic stress drop and its average value over the VW segment, respectively, and $\Delta\tau_{\mathrm{vs}}$ is the stress increase over the VS areas. Hence we can write

$$\int_{\mathrm{VS\ patch}} \Delta\tau_{\mathrm{vs}}(x)dx = \beta\Delta\tau_{\mathrm{vw}}D_{\mathrm{vw}} \; , \tag{S19}$$

where β is a model-dependent geometric factor that specifies the fraction of the stress transferred onto the VS patch (with the remainder being transferred onto the larger VS region adjacent to the ruptured VW segment). We use $\beta = 1/2$ for the 2D model and $\beta = W/(2W + 2D_{\mathrm{vw}}) = 1/6$ for the 3D model, respectively, by assuming that stress is transferred equally in all directions and that, in 3D, β is proportional to the perimeter of the VW segment that is contiguous with the VS patch.

We construct the non-dimensional parameter B as the ratio of the patch resistance (Eq. S12)

and representative stress increase provided by ruptures of VW segments (Eq. S19):

$$B = \frac{\Delta\tau_{\mathrm{prop}}D_{\mathrm{vs}}W}{\beta\Delta\tau_{\mathrm{vw}}D_{\mathrm{vw}}W} = \frac{\bar{\sigma}_{\mathrm{vs}}(a_{\mathrm{vs}} - \lambda^* b_{\mathrm{vs}})D_{\mathrm{vs}}\ln(V_{\mathrm{dyn}}/V_{\mathrm{i}})}{\beta\Delta\tau_{\mathrm{vw}}D_{\mathrm{vw}}} \ , \tag{S20}$$

where λ^* is given by Eq. (S13). For the 3D model, the seismogenic fault width W would multiply both the numerator and denominator of Eq. (S20) and hence parameter B remains the same. In computing parameter B, we estimate $\Delta\tau_{\mathrm{vw}}$ for each simulation by taking the average stress drop within a VW segment of one-segment ruptures from that simulation and set $\ln(V_{\mathrm{dyn}}/V_{\mathrm{i}}) = 20$ for all cases. We would expect seismic events to preferentially propagate through the patch if B is small. For larger value of B, we expect a smaller percentage of earthquakes to propagate through the patch.

As discussed in the main text, parameter B is indeed correlated with the probability P that an event that has ruptured one of the VW segments would propagate through the VS patch. Fig. S2 illustrates this using a number of 2D simulation examples. Panels (a-d) show the effect of the characteristic velocity strengthening $\bar{\sigma}(a_{\mathrm{vs}} - b_{\mathrm{vs}})$ and of the size D_{vs} of the VS patch on the probability P for four different cases in which other parameters, including parameters of the VW segments, are varied. The properties of the VS patch have a systematic effect on P when other parameters are fixed, as discussed in the main text. Comparison of panels (b-d) shows that properties of the VW segments also have a significant effect. However, all these results collapse, with some scatter, onto a single curve when we compute parameter B for all simulation represented by dots in Fig. S2a-d and plot the resulting values of B against the percentage P of two-segment ruptures (Fig. S2e). If the contribution of the breakdown work at the crack tip is ignored, or equivalently if $\lambda^* = 1$ is assumed, then the correspondence between B and P for most values of B remains good, except for small values of B (Fig. S2f), consistent with our earlier estimate.

S4 Interseismic coupling (ISC) derived from a spring-slider model

Here we analyze the relationship between interseismic coupling (ISC) and the model parameters based on a simple spring-slider model, for the cases of the VS patch acting as a permanent barrier ($P = 0$). This analysis explains why ISC is relatively high even for such cases, as shown in Fig. 4d, and motivates the dependence of ISC on the parameter B_{appr} that also governs the seismic behavior of the model. The spring-slider model illustrated in Fig. S3 is a plausible simplification of our model in that slip within the central velocity-strengthening (VS) patch is driven by plate loading as well as by motion of the neighboring velocity-weakening (VW) segments.

We consider periodic model behavior, in which the VW block has earthquakes every T years, with (instantaneous) slip $V_{\mathrm{pl}}T$, and the VS block responds in the interseismic period with both postseismic and interseismic slip. The quasi-static equation for the shear stress τ acting on the central block that represents the VS patch is given by

$$\tau = \tau_{\mathrm{i}} - (\delta - \delta_{\mathrm{vw}})k_{\mathrm{vw}} - (\delta - V_{\mathrm{pl}}t)k_{\mathrm{pl}} \ , \tag{S21}$$

where τ_{i} is the initial shear stress of the VS block, δ is the slip of the VS block, δ_{vw} is the

prescribed motion of the VW block that represents a VW segment, t is time, $V_{\mathrm{pl}}t$ is the motion of the block that represents plate loading, and k_{vw} and k_{pl} are stiffnesses associated with the springs that connect the VS block to the VW block and the loading block, respectively. For comparison with the continuum models, the spring stiffnesses can be written in the form μ/D, where μ is the shear modulus and D is the typical spatial scale over which the elastic interaction occurs. For the interaction between the creeping VS patch and the locked VW segment, we take the characteristic spatial scale as D_{vs}, since the locked region is adjacent to the VS patch. For the interaction between the creeping VS patch and the loading segments, the characteristic spatial scale is $(R + D_{\mathrm{vs}})$, where R is the distance between the VS patch and the fault areas that creep with the loading rate in our numerical models. Hence, we take:

$$k_{\mathrm{vw}} = \mu/D_{\mathrm{vs}} \ , \ k_{\mathrm{pl}} = \mu/(R + D_{\mathrm{vs}}) \ , \tag{S22}$$

where $R = D_{\mathrm{vw}}$ for the 2D model. For the 3D model, R is smaller, comparable to the seismogenic depth W.

Let $t = 0$ correspond to the end of one of the interseismic periods, so that one of the earthquakes experienced by the VW block occurs at $t = 0^+$. Then Eq. (S21) can be rewritten for $0^+ < t < T$ as

$$\tau = \tau_{\mathrm{i}} - \delta k_{\mathrm{vw}} - (\delta - V_{\mathrm{pl}}t)k_{\mathrm{pl}} + \Delta\tau_{\mathrm{vs}} \ , \tag{S23}$$

where $\Delta\tau_{\mathrm{vs}} = V_{\mathrm{pl}}Tk_{\mathrm{vw}}$ is the shear stress increase on the VS block due to the sudden slip of the VW block and $\delta(0^+) = \delta_{\mathrm{i}} = 0$.

The frictional strength τ_{str} of the VS block is:

$$\tau_{\mathrm{str}} = \tau_{\mathrm{i}} + \bar\sigma_{\mathrm{vs}}(a_{\mathrm{vs}} - b_{\mathrm{vs}})\ln(V/V_{\mathrm{i}}) \ , \tag{S24}$$

where V_{i} is the initial slip rate of the VS patch and it is assumed that the block remains in steady state throughout its motion as supported by our simulations. The equation of motion of the VS block is given by $\tau = \tau_{\mathrm{str}}$. The periodic behavior of the VS patch is enforced by requiring that

$$V(T) = V_{\mathrm{i}} \ , \tag{S25}$$

which leads to $\tau(T) = \tau_{\mathrm{f}}(T) = \tau_{\mathrm{i}}$ based on Eq. (S24) and $\delta(T) = V_{\mathrm{pl}}T$ based on Eq. (S21). Hence, in one period, all blocks in the model move by $V_{\mathrm{pl}}T$, as required for periodic behavior.

The mathematical form of a spring-slider problem similar to the one formulated here can be found elsewhere (*Perfettini and Avouac*, 2004). The resulting $\delta(t)$ and $V(t)$ are given by

$$\delta(t) \ = \ V_{\mathrm{f}}t_r \ln\left[1 + \Omega\frac{V_{\mathrm{i}}}{V_{\mathrm{f}}}(\exp(t/t_r) - 1)\right] \ , \tag{S26}$$

$$V(t) \ = \ V_{\mathrm{i}}\frac{\Omega\exp(t/t_r)}{1 + \Omega\frac{V_{\mathrm{i}}}{V_{\mathrm{f}}}[\exp(t/t_r) - 1]} \ , \tag{S27}$$

where

$$\Omega = \exp\left[\frac{\Delta\tau_{vs}}{\bar{\sigma}_{vs}(a_{vs}-b_{vs})}\right] , \tag{S28}$$

$$t_r = \frac{\bar{\sigma}_{vs}(a_{vs}-b_{vs})}{V_{pl}k_{pl}} , \tag{S29}$$

$$V_f = \frac{V_{pl}k_{pl}}{k_{vw}+k_{pl}} . \tag{S30}$$

From the periodic condition (Eq. S25), we obtain

$$V_i = \frac{V_f}{\Omega}\left(\frac{\Omega\exp(T/t_r)-1}{\exp(T/t_r)-1}\right) . \tag{S31}$$

Note that $V_f < V_{pl}$ since $k_{vw} > 0$ and $k_{pl} > 0$, and V_f gives the slip velocity of the VS block at which the stress changes on the VS block due to elastic interactions with the locked VW block and with the steadily moving loading block would exactly balance. Further, for $\Omega \gg 1$ and $T \gg t_r$ as typical for the range of parameters from the continuum models, $V_i \approx V_f$. The evolution of slip (Eq. S26) of the VS block predicts postseismic relaxation curves similar to those observed in the continuum models (Fig. 2f). An example of slip evolution given by Eq. (S26) for $\Omega = 100$ and $T/t_r = 6$ is plotted in Fig. S4a.

Let us now compute ISC of the VS block, which is determined by the slip deficit accumulated over the period when the VS block slides with slip velocity less than V_{pl}. Setting $V(t_{Vpl}) = V_{pl}$, where t_{Vpl} is the time at which the VS block slows down to V_{pl} (Fig. S4a), solving for t_{Vpl}, and finding the slip at time $t = t_{Vpl}$, we get:

$$\delta(t_{Vpl}) = V_f t_r \ln\left[\frac{V_f(\Omega-1)}{(1-\exp(-T/t_r))(V_{pl}-V_f)}\right] . \tag{S32}$$

The total slip in one period is given by

$$\delta(T) \equiv V_{pl}T = V_f t_r \left(\ln\Omega + T/t_r\right) . \tag{S33}$$

Hence

$$\text{ISC} = \frac{\delta(t_{Vpl})}{\delta(T)} = \frac{\ln(\Omega-1) - \ln[1-\exp(-T/t_r)] - \ln\left[(V_{pl}-V_f)/V_f\right]}{\ln\Omega + T/t_r} . \tag{S34}$$

We plot the ISC predicted by the spring-slider model for a range of the sizes D_{vs} of the VS patch, periods T observed in the 2D simulations, and the rate and state parameters $(a_{vs}-b_{vs})$ (Fig. S4b,c). The values of ISC shown in (Fig. S4b,c) are comparable to the ones obtained in the continuum simulations with $P = 0$ (Fig. 4b,d). In particular, the ISC is relatively high, larger than 0.6 for most parameter combinations, just as observed in the continuum simulations. In addition, Eq. (S34) predicts that ISC is lower for smaller R (Fig. S4d), consistent with the lower values of the ISC found in the 3D simulations compared to those in the 2D simulations (Fig. 4d). In the 3D model, the larger VS region adjacent to the top and bottom of the VS patch would act as a loading region, so that $R \approx W < D_{vw}$, leading to the lower values of ISC.

Let us simplify Eq. (S34) assuming the parameter regime motivated by the 2D continuum model, with $\Omega \gg 1$, $T \gg t_r$, and $R = D_{\text{vw}} \gg D_{\text{vs}}$. Then ISC is given by

$$\text{ISC} = 1 - \frac{\bar{\sigma}_{\text{vs}}(a_{\text{vs}} - b_{\text{vs}})D_{\text{vs}}}{V_{\text{pl}}T\mu} \ln\left(\frac{D_{\text{vw}}}{D_{\text{vs}}}\right) \ . \tag{S35}$$

Let us further assume that the coseismic slip of a VW segment is related to its average stress drop $\Delta\tau_{\text{vw}}$ through a quasi-static crack model, so that $V_{\text{pl}}T = D_{\text{vw}}\Delta\tau_{\text{vw}}/\mu$. Then

$$\text{ISC} = 1 - \frac{\bar{\sigma}_{\text{vs}}(a_{\text{vs}} - b_{\text{vs}})D_{\text{vs}}}{\Delta\tau_{\text{vw}}D_{\text{vw}}} \ln\left(\frac{D_{\text{vw}}}{D_{\text{vs}}}\right) \ . \tag{S36}$$

Eq. (S36) shows that ISC primarily depends on the quantity $F = \bar{\sigma}_{\text{vs}}(a_{\text{vs}} - b_{\text{vs}})D_{\text{vs}}/(\Delta\tau_{\text{vw}}D_{\text{vw}})$. This quantity also appears in the approximate expression B_{appr} for the non-dimensional parameter B that governs the seismic behavior of the continuum models. In fact, F and B_{appr} differ only by the geometric model-dependent parameter β which obviously cannot be captured by a spring-slider model. Hence this analysis motivates the dependence of ISC on B discussed in the main text.

References

Abercrombie, R. E., and J. R. Rice, Can observations of earthquake scaling constrain slip weakening?, *Geophys. J. Int., 162(2)*, 406–424, 2005.

Cocco, M., and A. Bizzarri, On the slip-weakening behavior of rate and state dependent constitutive laws, *Geophys. Res. Lett., 29(11)*, 2002.

Day, S. M., L. A. Dalguer, N. Lapusta, and Y. Liu, Comparison of finite difference and boundary integral solutions to three-dimensional spontaneous rupture, *J. Geophys. Res., 110*, 2005.

Dieterich, J. H., Time-dependent friction and the mechanics of stick-slip, *J. Geophys. Res., 116*, 790–806, 1978.

Dieterich, J. H., Modeling of rock friction: 1. Experimental results and constitutive equations, *J. Geophys. Res., 84*, 2,161–2,168, 1979.

Kaneko, Y., N. Lapusta, and J.-P. Ampuero, Spectral element modeling of spontaneous earthquake rupture on rate and state faults: Effect of velocity-strengthening friction at shallow depths, *J. Geophys. Res., 113*, 2008.

Lapusta, N., and Y. Liu, Three-dimensional boundary integral modeling of spontaneous earthquake sequences and aseismic slip, *J. Geophys. Res.*, 2009.

Lapusta, N., J. Rice, Y. Ben-Zion, and G. Zheng, Elastodynamic analysis for slow tectonic loading with spontaneous rupture episodes on faults with rate- and state-dependent friction, *J. Geophys. Res., 105*, 23,765–23,789, 2000.

Perfettini, H., and J. P. Avouac, Postseismic relaxation driven by brittle creep: A possible mechanism to reconcile geodetic measurements and the decay rate of aftershocks, applications to the Chi-Chi earthquake, Taiwan, *J. Geophys. Res., 109*, 2004.

Rice, J. R., Spatio-temporal complexity of slip on a fault, *J. Geophys. Res., 98*, 9,885–9,907, 1993.

Rubin, A. M., and J.-P. Ampuero, Earthquake nucleation on (aging) rate and state faults, *J. Geophys. Res., 110*, 2005.

Ruina, A. L., Slip instability and state variable friction laws, *J. Geophys. Res., 88*, 10,359–10,370, 1983.

Zheng, G., and J. R. Rice, Conditions under which velocity-weakening friction allows a self-healing versus a cracklike mode of rupture, *Bull. Seismol. Soc. Am., 88*, 1,466–1,483, 1998.

Table S1: The range of model parameters used to explore the correspondence between the non-dimensional parameter B and the model behavior (Fig. 4c,d).

| Parameter	Symbol	2D model	3D model
Shear modulus	μ	30, 60 GPa	30 GPa
Characteristic slip distance in VW	L_{vw}	8, 16, 24 mm	8 mm
Characteristic slip distance in VS	L_{vs}	4, 8, 16, 24 mm	8 mm
Effective normal stress in VW	$\bar{\sigma}_{\text{vw}}$	25, 50 MPa	50 MPa (mid-depth)
Effective normal stress in VS	$\bar{\sigma}_{\text{vs}}$	25, 50 MPa	50 MPa (mid-depth)
The size of the VW segment	D_{vw}	$30 - 100$ km	72.5 km
The size of the VS patch	D_{vs}	$5 - 50$ km	$5, 10, 15$ km
Rate and state parameter a in VW	a_{vw}	$0.005 - 0.025$	0.01
Rate and state parameter a in VS	a_{vs}	$0.01 - 0.02$	0.01
Rate and state parameter b in VW	b_{vw}	$0.005 - 0.030$	0.015
Rate and state parameter b in VS	b_{vs}	$0 - 0.020$	$0.005, 0.007, 0.009$
Seismogenic width	W	N/A	36.25 km
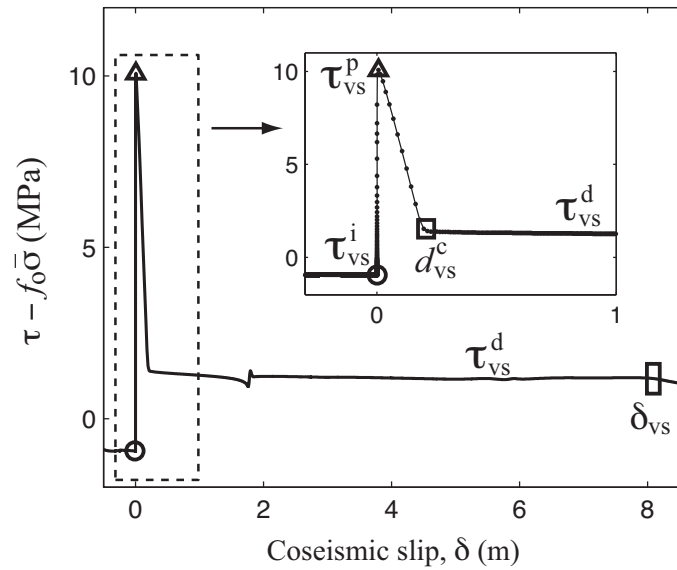
Figure S1: An example of shear stress evolution in the VS patch during coseismic slip. Shear stress τ with respect to a reference stress value $f_o\bar{\sigma}$ at the center of the VS patch ($x = 120$ km) is shown as a function of the coseismic slip of event 20 in Fig. 2b. The open circle indicates the stress τ_{vs}^i before the arrival of the dynamic rupture. The open triangle shows the peak shear stress τ_{vs}^p. The open square and the rectangle correspond to effective weakening distance d_{vs}^c and the amount of coseismic slip δ_{vs}, respectively.
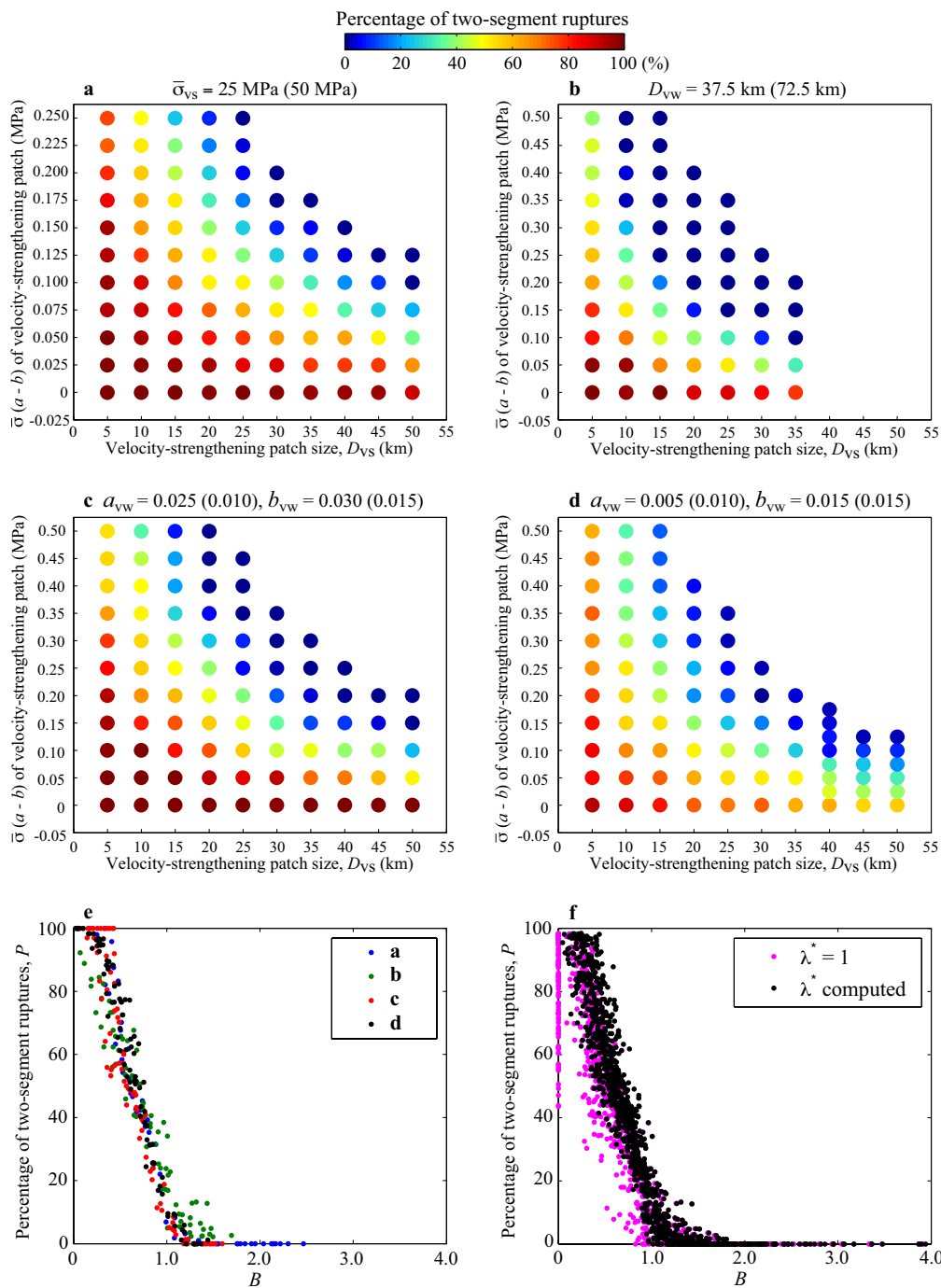
Figure S2: Additional simulation results illustrating how non-dimensional parameter B captures the behavior of the 2D model as its parameters are varied. (a-d) The dependence of the percentage P of two-segment ruptures on the properties of the VS patch as other model parameters are varied with respect to the simulations shown in Fig. 4a. In Fig. 4a, the following parameters are used: $\bar{\sigma}_{vw} = \bar{\sigma}_{vs} = 50$ MPa, $a_{vw} = 0.010$, $b_{vw} = 0.015$, and $D_{vw} = 72.5$ km. Panels (a-d) show results for a set of simulations with one or two of these parameters modified, as indicated at the top of each panel. The numbers in parentheses indicate the parameters in Fig. 4a. Comparison of panels (b-d) illustrates that the parameters of the VW segments also play an important role. (e) Relation between the percentage of two-segment ruptures P and the non-dimensional parameter B for cases in panels (a-d). The results collapse, with some scatter, onto a single curve. (f) Relation between P and B with (black dots) and without (purple dots) taking into account breakdown work in the estimate of B. Each dot corresponds to an earthquake sequence with different combination of model parameters as given by Table S1.
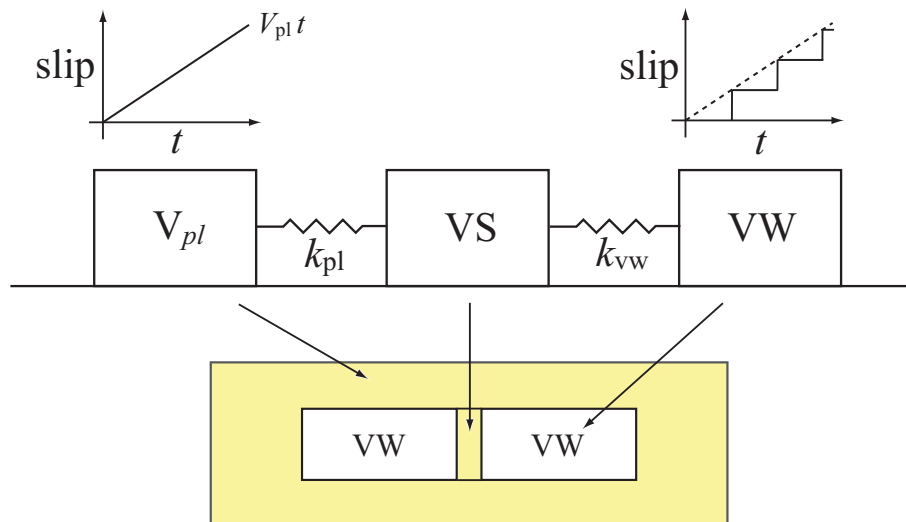
Figure S3: A sketch illustrating the spring-slider system used to estimate ISC. The velocity-strengthening (VS) block in the middle represents the VS patch in the continuum models. The motion of the VS block is driven by the prescribed steady and stick-slip motions of the loading block and the VW block, respectively.
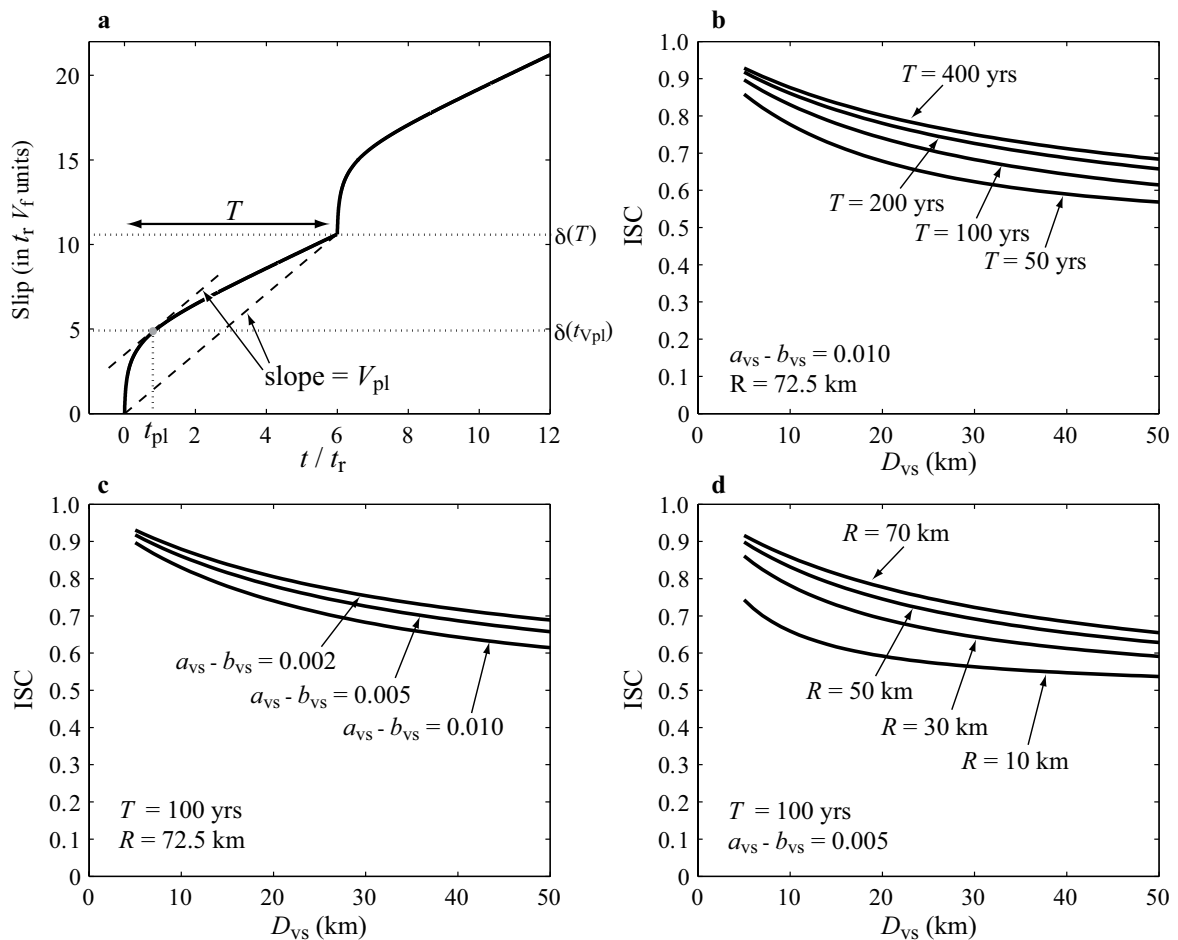
Figure S4: Behavior of the velocity-strengthening (VS) block in the spring-slider model illustrated in Fig. S3. We assume that $k_{vw} = \mu/D_{vs}$ and $k_{pl} = \mu/(R + D_{vs})$ as discussed in the text and take $\mu = 30$ GPa, $V_{pl} = 5$ cm/s, and $\sigma_{vs} = 50$ MPa, the same values as for the continuum models. (a) Slip as a function of time for two earthquake cycles of the model, as given by Eq. (S26). (b-d) The dependence of interseismic coupling (ISC) given by Eq. (S34) on the interseismic period T, the rate-and-state parameter $a_{vs} - b_{vs}$, and the typical interaction distance R that determines the spring stiffness k_{pl} between the VS block and the loading block.

Online Supplementary Movie for

Towards inferring earthquake patterns from geodetic observations of interseismic coupling

Nature Geoscience 2010

Yoshihiro Kaneko, Jean-Philippe Avouac, Nadia Lapusta

March 17, 2010

Movie S1: 3D simulation example of long-term fault behavior due to interaction of two seismogenic velocity-weakening (VW) segments separated by a velocity-strengthening (VS) patch. The VS patch creates complexity of large events in the model, acting as an occasional barrier to seismic rupture and causing clustering of large events. The VW segments and VS patch are surrounded by a larger VS region; the boundaries between areas of different friction properties are shown as white lines. The simulated time t is shown at the top in years. Colors represent slip rate on the fault, with seismic slip rates shown in white and bright yellow, postseismic slip and interseismic creep shown in orange and red, and locked portions shown in black. The interframe rate of the movie is variable, from several years in the interseismic period to several seconds during dynamic rupture propagation. The potency deficit is defined as $V_{\mathrm{pl}}tA - \int_A \delta dA$, where V_{pl} is the plate rate, δ is the accumulated slip, and A is the area of the region $-92 \text{ km} \leq X \leq 92 \text{ km}$ and $-25 \text{ km} \leq Z \leq 25 \text{ km}$. The 6th simulated earthquake starts shortly after $t = 200$ years and ruptures both VW segments and the central VS patch. After the earthquake, the VS fault areas experience postseismic slip. In the interseismic period, the two VW segments are locked and the surrounding VS region is creeping. The creep is slowly penetrating into the locked regions due to stress concentrations between the creeping and locked areas. At $t = 229$ years, the 7-th event starts at the same location as the 6-th one but arrests at the VS patch. The resulting postseismic slip triggers the smaller 8-th and 9-th earthquakes about 9 and 10 days later, respectively. This leads to a complex pattern of smaller seismic events and aseismic transients in the right VW segment between $t = 230$ and $t = 266$ years. The potency deficit shows that the model is neither time-predictable nor slip-predictable. In the interseismic periods, the VS patch has slip rates of the order of 3×10^{-10} m/s, lower than the plate rate of 5 cm/yr $= 1.6 \times 10^{-9}$ m/s and corresponding to interseismic coupling of 0.80.